ARTICLE

Comprehensive analysis of the chromatin landscape in *Drosophila melanogaster*

Peter V. Kharchenko[1,2], Artyom A. Alekseyenko[3,4], Yuri B. Schwartz[5]†, Aki Minoda[6], Nicole C. Riddle[7], Jason Ernst[8,9], Peter J. Sabo[10], Erica Larschan[3,4,11], Andrey A. Gorchakov[3,4], Tingting Gu[7], Daniela Linder-Basso[5]†, Annette Plachetka[3,4], Gregory Shanower[5]†, Michael Y. Tolstorukov[1,2], Lovelace J. Luquette[1], Ruibin Xi[1], Youngsook L. Jung[1,3], Richard W. Park[1,12], Eric P. Bishop[1,12], Theresa P. Canfield[10], Richard Sandstrom[10], Robert E. Thurman[10], David M. MacAlpine[13], John A. Stamatoyannopoulos[10,14], Manolis Kellis[8,9], Sarah C. R. Elgin[7], Mitzi I. Kuroda[3,4], Vincenzo Pirrotta[5], Gary H. Karpen[6]* & Peter J. Park[1,2,3]*

Chromatin is composed of DNA and a variety of modified histones and non-histone proteins, which have an impact on cell differentiation, gene regulation and other key cellular processes. Here we present a genome-wide chromatin landscape for *Drosophila melanogaster* based on eighteen histone modifications, summarized by nine prevalent combinatorial patterns. Integrative analysis with other data (non-histone chromatin proteins, DNase I hypersensitivity, GRO-Seq reads produced by engaged polymerase, short/long RNA products) reveals discrete characteristics of chromosomes, genes, regulatory elements and other functional domains. We find that active genes display distinct chromatin signatures that are correlated with disparate gene lengths, exon patterns, regulatory functions and genomic contexts. We also demonstrate a diversity of signatures among Polycomb targets that include a subset with paused polymerase. This systematic profiling and integrative analysis of chromatin signatures provides insights into how genomic elements are regulated, and will serve as a resource for future experimental investigations of genome structure and function.

The model organism Encyclopedia of DNA Elements (modENCODE) project is generating a comprehensive map of chromatin components, transcription factors, transcripts, small RNAs and origins of replication in *Drosophila melanogaster* and *Caenorhabditis elegans*[1,2]. *Drosophila* has been used as a model system for over a century to study chromosome structure and function, gene regulation, development and evolution. The availability of high-quality euchromatic and heterochromatic sequence assemblies[3–5], extensive annotation of functional elements[6], and a vast repertoire of experimental manipulations enhance the value of epigenomic studies in *Drosophila*.

Genome-wide profiling of chromatin components provides a rich annotation of the potential functions of the underlying DNA sequences. Previous work has identified patterns of post-translational histone modifications and non-histone proteins associated with specific elements (for example, transcription start sites, enhancers), as well as delineating the transcriptional status of genes and large domains[7,8]. Here we present a comprehensive picture of the chromatin landscape in a model eukaryotic genome. We define combinatorial chromatin 'states' at different levels of organization, from individual regulatory units to the chromosome level, and relate individual states to genome functions.

Combinatorial chromatin states

We performed chromatin immunoprecipitation (ChIP)-array analysis for numerous histone modifications and chromosomal proteins

(Supplementary Table 1), using antibodies tested for specificity and cross-reactivity[9] (Supplementary Fig. 1). Here we describe analyses of cell lines S2-DRSC (S2) and ML-DmBG3-c2 (BG3), derived from late male embryonic tissues (stages 16–17) and the central nervous system of male third instar larvae, respectively (see http://www.modencode.org for data from other cell lines and animal stages). Analysis reveals groups of correlated features, including those associated with heterochromatic regions[10], Polycomb-mediated repression[11], and active transcription[12] (Supplementary Fig. 2), similar to those observed in other organisms[13,14]. This indicates that specific histone modifications work together to achieve distinct chromatin 'states'.

We used a machine-learning approach to identify the prevalent combinatorial patterns of 18 histone modifications, capturing the overall complexity of chromatin profiles observed in S2 and BG3 cells with 9 combinatorial states (Fig. 1a, Methods). The model associates each genomic location with a particular state, generating a chromatin-centric annotation of the genome (Fig. 1b). We examined each state for enrichment in non-histone proteins (Fig. 1a and Supplementary Fig. 3) and gene elements, as well as distribution across the karyotype (Fig. 1b and Supplementary Fig. 4) and finer-scale levels (Fig. 1c–e).

Most distinct chromatin states are associated with transcriptionally active genes. Active promoter and transcription start site (TSS)-proximal regions are identified by state 1 (Fig. 1; red), marked by prominent enrichment in H3K4me3/me2 (tri/dimethylation of residue K4 of
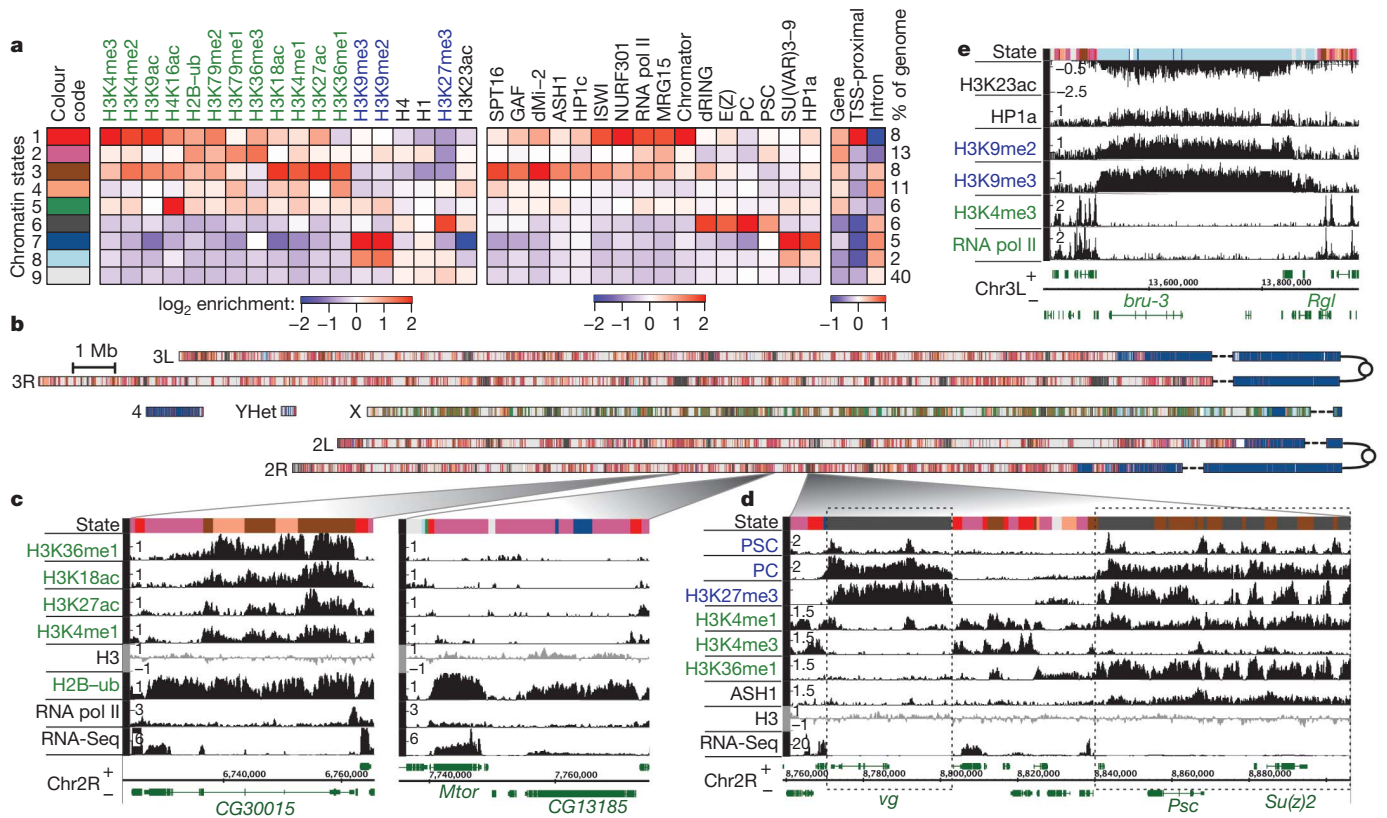
Figure 1 | Chromatin annotation of the *Drosophila melanogaster* genome.
a, A 9-state model of prevalent chromatin states found in S2 and BG3 cells. Each chromatin state (row) is defined by a combinatorial pattern of enrichment (red) or depletion (blue) for specific chromatin marks (first panel, columns; active marks in green, repressive in blue). For instance, state 1 is distinguished by enrichment in H3K4me2/me3 and H3K9ac, typical of transcription start sites (TSS) in expressed genes. The enrichments/depletions are shown relative to chromatin input (S2 data shown, see Supplementary Fig. 3 for BG3 data and histone density normalization). The second panel shows average enrichment of chromosomal proteins. The third panel shows fold over/under-representation of genic and TSS-proximal (±1 kb) regions relative to the entire tiled genome. The enrichment of intronic regions is relative to genic regions associated with each state. **b**, A genome-wide karyotype view of the domains defined by the 9-state model in S2 cells. Centromeres are shown as open circles, and dashed lines span gaps in the genome assembly. Several prominent chromatin organization features are illustrated (colour code in **a**), including the extent of pericentromeric heterochromatin (state 7) and the H4K16ac-driven signature of the dosage-compensated male X chromosome (state 5). (BG3 in Supplementary Fig. 4.) **c–e**, Examples of chromatin annotation at specific loci. **c**, Two distinct chromatin signatures of transcriptionally active genes: one (left) is associated with enrichment in marks of states 3 and 4, whereas the other (right) is limited to states 1 and 2, recapitulating well established TSS and elongation signatures (note that small patches of state 7 in CG13185 illustrate H3K9me2 found at some expressed genes in S2 cells[16]). **d**, A locus containing two Polycomb-associated domains, silent (left) and balanced (right). **e**, A large state 8 domain located within euchromatic sequence in BG3 cells, enriched for chromatin marks typically associated with heterochromatic regions, but at lower levels than in pericentromeric heterochromatin (state 7).

histone H3) and H3K9ac (acetylation of K9 of histone H3). The transcriptional elongation signature associated with H3K36me3 enrichment is captured by state 2 (purple), found preferentially over exonic regions of transcribed genes. State 3 (brown), typically found within intronic regions, is distinguished by high enrichment in H3K27ac, H3K4me1 and H3K18ac. A related chromatin signature is captured by state 4 (coral), distinguished by enrichment of H3K36me1, but notably lacking H3K27ac. The number of genes associated with each chromatin state and the distribution of states within genes are shown in Supplementary Fig. 5.

Several aspects of large-scale organization are revealed by the karyotype view (Fig. 1b). Chromosome X is markedly enriched for state 5 (green), distinguished by high levels of H4K16ac in combination with H3K36me3 and other marks of 'elongation' state 2 (a combinatorial pattern associated with dosage compensation in male cells[15]). Pericentromeric heterochromatin domains and chromosome 4 are characterized by high levels of H3K9me2/me3 (state 7, dark blue)[10]. Finally, the model distinguishes another set of heterochromatin-like regions containing moderate levels of H3K9me2/me3 (state 8, light blue; Fig. 1e). Surprisingly, this state occupies extensive domains in autosomal euchromatic arms in BG3 cells, and in chromosome X in both cell lines[16].

Further aspects of chromatin organization can be visualized by folding the chromosome using a Hilbert curve (Fig. 2a)[17], which maintains the spatial proximity of nearby elements. Thus, local patches of corresponding colours reveal the sizes and relative positions of domains associated with particular chromatin states (Fig. 2b and Supplementary Figs 6–9). For instance, specks of TSS-proximal regions (state 1) are typically contained within larger blocks of transcriptional elongation marks (state 2), which are in turn encompassed by extensive patches of H3K36me1-enriched domains (state 4) and variable-sized blocks of state 3. The clusters of open chromatin formed by these gene-centric patterns are separated by extensive silent domains (state 9) and regions of Polycomb-mediated repression (state 6). Factors responsible for domain boundaries were not identified in our analysis (Supplementary Fig. 10).

We also developed a multi-scale method to characterize chromatin organization at the spatial scale appropriate for the genome properties being investigated. For example, we observe that chromatin patterns most accurately reflect the replication timing of the S2 genome at scales of ~170 kb (Supplementary Information, section 1). This is consistent with size estimates of chromatin domains influencing replication timing[18], and suggests that multiple replication origins are coordinately regulated by the local chromatin environment (each replicon is ~28–50 kb[19]).

To examine combinatorial patterns not distinguished by the simplified 9-state model, we also generated a 30-state combinatorial model that uses presence/absence probabilities of individual marks[20] (Supplementary
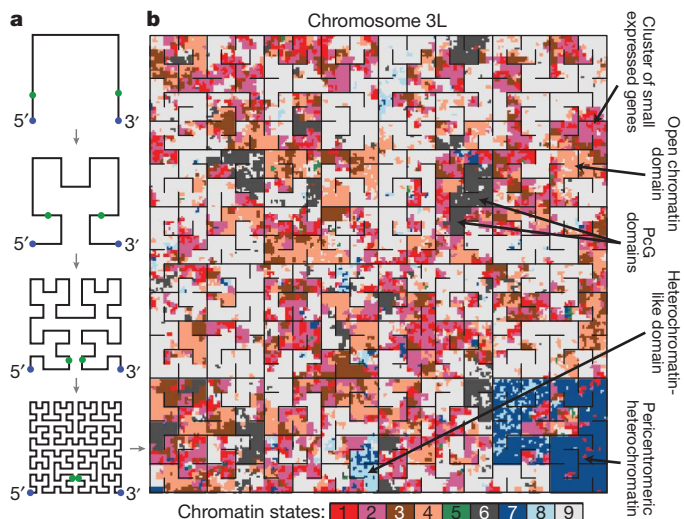
Figure 2 | Visualization of spatial scales and organization using compact folding. a, The chromosome is folded using a geometric pattern (Hilbert space-filling curve) that maintains spatial proximity of nearby regions. An illustration of the first four folding steps is shown. Note that although this compact curve is optimal for preserving proximity relationships, some distal sites appear adjacent along the fold axis (green dots). **b,** Chromosome 3L in S2 cells. A domain of a given chromatin state appears as a patch of uniform colour of corresponding size. Thin black lines are used to separate regions that are distant on the chromosome. The folded view illustrates chromatin organization features that are not easily discerned from a linear view: active TSSs (state 1) appear as small specks surrounded by elongation state 2, commonly next to larger regions marked by H3K36me1-driven state 4, which also contains patches of intron-associated state 3. These open chromatin regions are separated by extensive domains of state 9. See Supplementary Figs 6 and 7 for other chromosomes and BG3 data. The folded views can be browsed alongside the linear annotations and other relevant data online: http://compbio.med.harvard.edu/flychromatin.

Fig. 11). The increased number of states can identify finer variations that are biologically significant, for example, a signature corresponding to transcriptional elongation in heterochromatic regions[16].

Chromatin state variation among genes

Active genes generally display enrichments or depletions of individual marks at specific gene segments (Fig. 3a). When classified according to their chromatin signatures (Supplementary Fig. 12), active genes fall into subclasses correlated with expression magnitude (Supplementary Information, section 2), gene structure and genomic
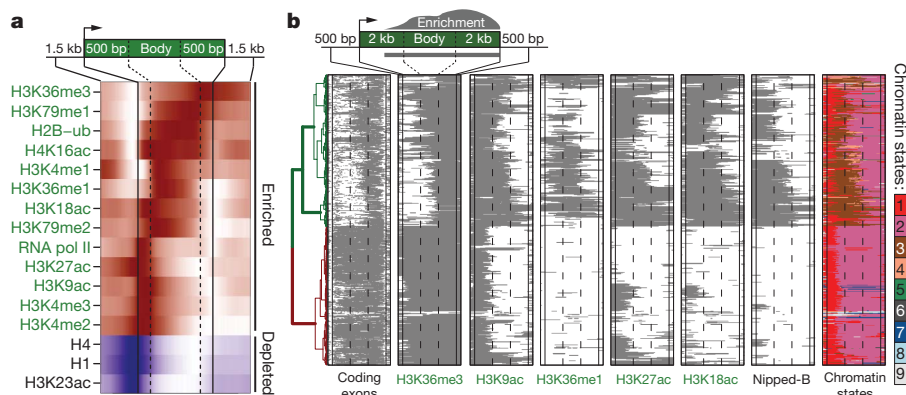
context (for example, heterochromatic genes combine H3K9me2/me3 with some active marks)[16]. Of particular interest is one class of long expressed genes, many with regulatory functions, which are enriched for H3K36me1 (cluster 2, Supplementary Fig. 12; 131 genes in S2, 202 in BG3; Supplementary Table 2).

To examine further the patterns associated with long genes, we clustered expressed autosomal genes ≥4 kb based on blocks of enrichment for each chromatin mark (Fig. 3b; 1,055 genes). We observe that genes with large 5′-end introns (green subtree, Fig. 3b; 552 genes) show extensive H3K27ac and H3K18ac enrichment, broader H3K9ac domains, and blocks of H3K36me1 enrichment (chromatin state 3, Fig. 3b, last column). These genes are enriched for developmental and regulatory functions (Supplementary Table 3), and are positioned within domains of Nipped-B[21] (Fig. 3b), a cohesin-complex loading protein previously associated with transcriptionally active regions[21,22]. In contrast, genes with more uniformly distributed coding regions (red subtree, Fig. 3b) lack most state 3 marks, and H3K9ac enrichment is restricted to the 2 kb downstream of the TSS. These differences are not explained by variation in histone density (Supplementary Fig. 13). Overall, the presence or absence of state 3 is the most common difference in the chromatin composition of expressed genes that are 1 kb and longer (Supplementary Fig. 14), and the presence of state 3 consistently correlates with a reduced fraction of coding sequence in the gene body, mainly associated with the presence of a long first intron.

State 3 domains are highly enriched for specific chromatin remodelling factors (SPT16 (also known as DRE4) and dMI-2; Supplementary Figs 15 and 16), whereas state 1 regions around active TSSs are preferentially bound by NURF301 (also called E(bx)) and MRG15. ISWI is enriched in both states 1 and 3 (Supplementary Figs 16 and 17). State 3 domains also exhibit the highest levels of nucleosome turnover[23], and show higher enrichment of the transcription-associated H3.3 histone variant[24] than either the TSS- or elongation-associated states 1 and 2 (Supplementary Figs 15 and 16). Consistent with earlier analyses of cohesin-bound regions[25], state 3 sequences tend to replicate early in G1 phase, and show abundance of early replicating origins (Supplementary Fig. 18). A regulatory role for state 3 domains is suggested by enrichment for a known enhancer binding protein (dCBP/p300[26]) in adult flies, and for enhancers validated in transgene constructs[27] (Supplementary Fig. 19).

Modes of regulation in Polycomb domains

In *Drosophila*, loci repressed by Polycomb group (PcG) proteins are embedded in broad H3K27me3 domains that are regulated by Polycomb response elements (PREs) bound by E(Z), PSC and dRING (Fig. 1d)[28,29]. We find that regions of H3K4me1 enrichment surround all

Figure 3 | Chromatin patterns associated with transcriptionally active genes. a, Location and extent of chromatin features relative to boundaries of expressed genes (≥1 kb) in BG3 cells. The colour intensity indicates the relative frequency of enrichment/depletion (red/blue) of a given mark within the gene (normalized independently for each mark). **b,** Regions enriched for 'active' chromatin marks in long transcribed genes. The plot shows the extent of regions enriched for various active marks at transcriptionally active genes (≥4 kb) on

BG3 autosomes. Each row represents a scaled gene. The first column illustrates coding exons; the last column shows chromatin state annotation. The clustering of the genes according to the spatial patterns of chromatin marks separates genes with a high fraction of coding sequence (red subtree, bottom) from genes containing long introns (green subtrees, top), which are associated with chromatin state 3 (last column) and binding of specific chromosomal proteins, such as Nipped-B[21] (also see Supplementary Fig. 13).

PREs, 90% of which also display narrower peaks of H3K4me2 enrichment (Supplementary Fig. 20). Although this pattern is reminiscent of transcriptionally active promoter regions, PREs lack H3K4me3, indicating that a different mechanism of H3K4 methylation is used, perhaps involving the Trithorax H3K4 histone methyltransferase (HMTase) found at all PREs[29].

To examine chromatin states associated with PcG targets, we analysed the chromatin and transcriptional signatures of TSSs in Polycomb-bound domains (Fig. 4a and Supplementary Fig. 21). In addition to fully repressed TSSs (cluster 1, Fig. 4a), we identify TSSs maintained in the 'balanced' state[29] (cluster 2, Fig. 4a), distinguished by coexistence of Polycomb with active marks (including the HMTase ASH1) and production of full-length messenger RNA transcripts (for example, *Psc* domain, Fig. 1d).

TSSs in clusters 3 and 4 are distinguished by the presence of adjacent PREs (Fig. 4a). Surprisingly, 53% of the PRE-proximal TSSs produce short RNA transcripts[30] (cluster 3, Fig. 4a), indicating stalling of engaged RNA pol II[30]. Using the global run-on sequencing (GRO-Seq) assay to accurately assess engaged RNA polymerases[31], we observe that cluster 3 TSSs produce short transcripts in the sense orientation. The level of GRO$^+$ signal is similar to that found at fully transcribed genes (Supplementary Fig. 22); thus, some transcription initiates in cluster 3, but elongation fails. Interestingly, these genes are enriched for regulatory and developmental functions, even more than other genes within Polycomb domains (see Supplementary Tables 4 and 5). Genes without TSS-proximal PREs generally lack short transcript signatures (for example, cluster 1 in Fig. 4a; see Supplementary Fig. 21 for exceptions). Importantly, engaged polymerases and transcripts are not a general feature of PREs; TSS-distal PREs typically lack short RNA and GRO-Seq signals (Fig. 4b and Supplementary Fig. 22) despite being similarly enriched in H3K4me1/me2. The striking link between TSS-proximal PREs and the production of short RNAs suggests a potential mechanism for control of these developmental regulatory genes, whereby the same features that recruit H3K4 methyl marks to PREs may also facilitate RNA pol II recruitment to nearby TSSs.

DHS plasticity and chromatin states

We used a DNase I hypersensitivity assay[32,33] to examine the distributions of putative regulatory regions and their relationships with chromatin states. DNase I hypersensitivity mapping broadly identifies sites with low nucleosome density and regions bound by non-histone proteins[34–36]. Short-read sequencing identified 8,616 high-magnitude DNase I hypersensitive sites (DHSs) in S2 cells and 6,354 in BG3 cells (and a comparable number of low-magnitude DHSs; Supplementary Fig. 23 and Methods). Approximately half of the high-magnitude DHSs are found at transcriptionally active TSSs (Supplementary Fig. 24). Thus, the chromatin context of the TSS-proximal DHSs is dominated by the features expected for an active TSS, including RNA pol II, H3K4me3 and other state 1 marks (clusters 1, 2; Fig. 5a and Supplementary Fig. 25).

Of the 36% TSS-distal DHSs, most (60%) are positioned within annotated expressed genes (Supplementary Fig. 24). These gene-body DHSs are distinguished from TSS-proximal DHSs by low H3K4me3, higher levels of H3K4me1, H3K27ac, and other marks linked to chromatin state 3 (clusters 3, 4; Fig. 5a and Supplementary Fig. 26). An additional 20% of the TSS-distal DHSs are outside of annotated genes, but show signatures associated with active transcription starts or elongation, suggesting new alternative promoters or unannotated genes (Supplementary Figs 27 and 28). The remaining 20% of TSS-distal DHSs that appear to be intergenic (6% of all DHSs) are typically enriched for H3K4me1, but lack other active marks (cluster 5, Fig. 5a).

Most DHS positions fall into the TSS-proximal state 1 or the intron-biased state 3 (Fig. 5b). State 3 lacks H3K4me3 and is enriched for H3K4me1, H3K27ac and H3K18ac, similar to mammalian enhancer elements[37]. Many state 3 DHS positions are occupied by known regulatory proteins: GAGA factor binds to 49% of these DHSs in S2 cells, and developmental transcription factors bind to 44% of these DHSs in embryos[38]. Notably, we find that TSS-distal DHSs in *Drosophila* exhibit low-level bi-directional transcripts (Fig. 5a, shortRNA panel; see also Supplementary Figs 29 and 30), analogous to the enhancer RNAs (eRNAs) characterized in mice[39]. Analysis of GRO-Seq data (Fig. 5e) indicates that eRNA-like transcripts are common to both intra- and intergenic TSS-distal DHSs in *Drosophila*, a feature that is conserved with mammals.

The association of DHSs with chromatin states 1 and 3 (Fig. 5c) persists even in chromosome 4 and pericentromeric heterochromatin, where such states are infrequent (Supplementary Fig. 31). This suggests that these chromatin states and associated remodelling factors (for example, ISWI, SPT16) provide the context necessary for non-histone chromosomal protein binding at DHSs, or are the consequence of such binding events. To investigate this interdependency, we analysed a high-confidence set of loci that exhibit DHSs in only one of the two examined cell lines (Supplementary Fig. 32). Surprisingly, although in general more DHSs are in state 1 regions, 91% of the cell-type-specific DHSs are found within state 3 domains (14-fold increase compared to state 1 DHSs; Supplementary Table 6 and Fig. 5d). Comparison with DHSs in an additional cell type (Kc167, Supplementary Fig. 33) confirms that DHSs displaying plasticity between cell types are mostly found in state 3. When DHSs are absent, the altered loci maintain chromatin state 3 in 23% of the cases (Fig. 5d), indicating that the presence of state 3 is not always dependent on the DHS. More frequently, the altered loci transition to state 4 (43% of the cases), an open chromatin state that lacks many of the histone modifications and chromatin remodellers characteristic of state 3. Although the less frequent
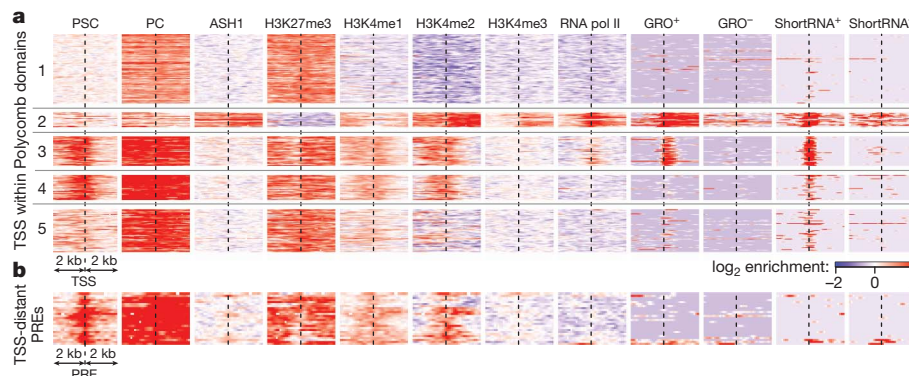

Figure 4 | Signatures of TSSs within domains of Polycomb-mediated repression. a, Distinct classes of TSSs in S2 cell Polycomb domains. Each row represents a TSS. Clusters 1–5 illustrate distinct TSS states (see Supplementary Fig. 21 for complete set of clusters). Cluster 1 shows fully repressed TSSs with the expected pattern of PC and H3K27me3 enrichment; cluster 2 shows 21 TSSs found within ASH1 domains, maintained in a balanced state. Clusters 3 and 4 distinguish TSSs located in the immediate proximity of Polycomb response elements (PREs), showing the symmetrical H3K4me1/me2 enrichment typical of all PREs. Many such TSSs (cluster 3, 42 TSSs) produce short, non-polyadenylated transcripts along the sense strand (GRO$^+$/shortRNA$^+$ columns), indicating the presence of paused polymerase. **b**, PRE positions distant from annotated TSSs. TSS-distal PREs exhibit enrichment for H3K4me1/me2, but are not associated with GRO or shortRNA signatures.
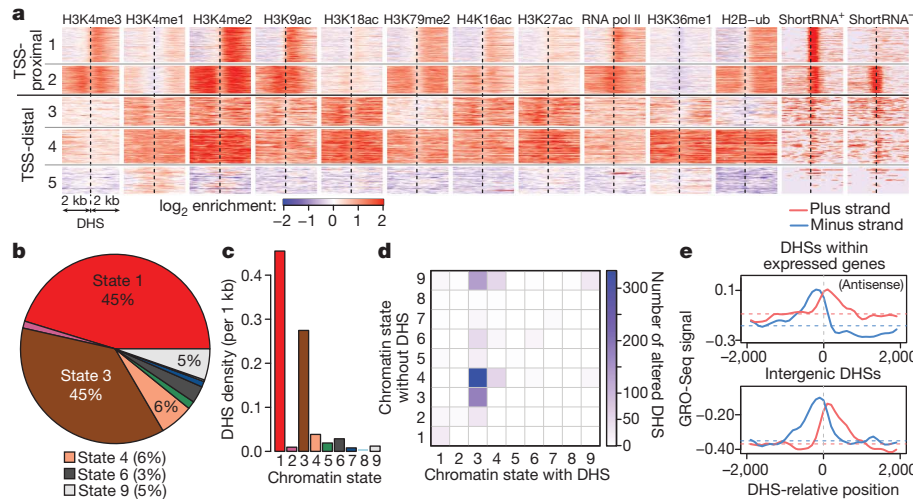
Figure 5 | Chromatin signatures of regulatory elements identified by DNase I hypersensitivity. a, Representative classes of high-magnitude DNase I hypersensitive sites (DHSs) and chromatin signatures in S2 cells. TSS-proximal (within 2 kb) DHSs show chromatin signatures expected of expressed gene promoters: high H3K4me3 and RNA pol II signal extending in the direction of transcription (left to right; cluster 2 groups bi-directional promoters). TSS-distal DHSs are associated with high H3K4me1 and low H3K4me3 levels. Most TSS-distal DHSs found within the bodies of expressed genes (clusters 3, 4) are associated with chromatin state 3. A cluster of rare intergenic DHSs (cluster 5) is associated with localized peaks of H3K4me1/2 (complete sets of clusters in Supplementary Figs 25, 26 and 28). b, Distribution of DHS positions among chromatin states. The vast majority of DHSs are found within the TSS-proximal state 1 or enhancer-like state 3 regions. c, States 1 and 3 exhibit the highest

density of DHSs. d, Cell-line-specific DHSs are positioned predominantly within the enhancer-like state 3. The transition matrix shows the chromatin state of loci containing DHSs in one cell line (x axis), and the state of the same locus in the other cell line where the DHS is absent (y axis). Most of the DHSs that differ between cell lines originate from state 3. When DHSs are absent, the loci typically transition to an open chromatin state 4 (43%), or maintain state 3 (23%). In both scenarios, most of the associated genes remain transcriptionally active (see Supplementary Fig. 34). e, Low levels of engaged RNA polymerase are associated with TSS-distal DHSs. The top plot shows the local increase in the antisense GRO-Seq signal for DHSs located within transcribed genes; dashed lines show median levels. Intergenic DHS positions (bottom plot) also show bi-directional GRO-Seq signal of comparable magnitude. See Supplementary Figs 27, 29 and 30.

transitions to the Polycomb state 6 (7%) or background state 9 (17%) typically coincide with gene silencing, most of the genes that maintain state 3 or transition to state 4 remain transcriptionally active (Supplementary Fig. 34). These observations provide further support for an enhancer-like function for state 3 DHSs, and suggest a more subtle regulatory role than simple linkage to the presence or absence of gene expression.

Chromatin annotation of genome functions

The genomic chromatin state annotation and discovery of refined chromatin signatures for chromosomes, domains, and subsets of regulatory genes demonstrate the utility of a systematic, genome-wide profiling of an organism that is already understood in considerable detail. Clearly, the definition and functional annotation of chromatin patterns will be enhanced by incorporation of data for different types of components. Five 'colours' of chromatin were recently identified in Kc167 cells using chromosomal protein maps[40]. Comparison with our 9-state model shows similarities as well as differences in the ability to distinguish functional elements (Supplementary Fig. 35); thus, further integration of such data in the same cell type may resolve additional functional features. Our results illustrate the utility of integrating multiple data types (histone marks, non-histone proteins, chromatin accessibility, short RNAs and transcriptional activity) for comprehensive characterization of functional chromatin states.

An important, repeated theme is that chromatin state analysis identifies unexpected distinctions between subsets of active genes. Besides the differences linked to genomic context (for example, male X chromosome, heterochromatin), the main source of variability is the presence of the acetylation-rich state 3 (Fig. 6). Several lines of evidence suggest that the intronic positions marked by state 3 are important for gene regulation. State 3 regions show specific associations with known chromatin remodellers (SPT16, dMi-2 and ISWI) and gene regulatory proteins (for example, GAF, dCBP/p300), and the highest rates of nucleosome turnover and transcription-dependent deposition of the H3.3 variant. State 3 genes are also bound by cohesin

complex proteins, thought to associate with decondensed chromatin[21] to promote looping interactions with promoter regions[22].

A regulatory role for state 3 chromatin is further suggested by the high density of DHSs, comparable to that of active TSS state 1, and the fact that state 3 accounts for most of the DHS plasticity among cell types. The combinations of histone marks found in state 3 are similar to signatures of mammalian enhancers[37], which also show high variability between cell types[37]. Furthermore, state 3 DHSs exhibit low levels of short, non-coding bidirectional transcripts reminiscent of eRNAs identified in mice[39]. Together, these findings suggest that state 3 regions contain enhancers or other regulatory elements, and that a combination of modifications can be used to identify new elements in the genome.

Genes within repressive Polycomb domains also display several distinct combinatorial chromatin patterns (Fig. 4a), which probably represent a range of functional states: repressed, paused, or expressed genes in either balanced[29] or fully activated states. Alternatively, distinct signatures might mark subsets of regulatory genes that require either long-term repression or the ability to reverse functional states, depending on environmental or developmental cues. The PRE-proximal paused TSSs have some similarity to the 'bivalent' genes in mammalian cells, which also display transcriptional pausing of key regulatory and developmental genes[41,42]. However, the mammalian 'bivalent state' is characterized by the simultaneous
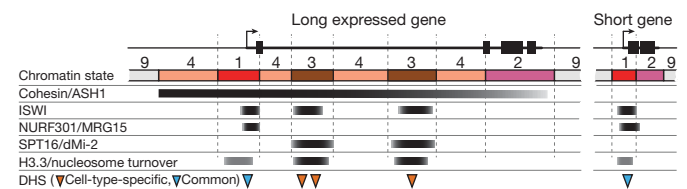

Figure 6 | Spatial arrangements of chromatin states associated with active transcription. Unlike short or exon-rich expressed genes, expressed genes with long intronic regions commonly contain one or more regions of enhancer-like state 3, associated with specific chromosomal proteins, high nucleosome turnover and DHSs displaying cell-type plasticity.

presence of PcG proteins, H3K27me3 and H3K4me3, which in *Drosophila* is found only in the fully elongating 'balanced' state[29,43].

Comprehensive analysis of chromatin signatures has enormous potential for annotating functional elements in both well studied and new genomes. Going forward, our systematic characterization of the epigenomic and transcriptional properties of *Drosophila* cells should spur in-depth experimental analyses of the relationship between chromatin states and genome functions, ranging from whole chromosomes down to individual regulatory elements and circuits.

METHODS SUMMARY

Histone modification and chromosomal protein antibodies were characterized for cross-reactivity. ChIP-chip was performed in duplicate, using Affymetrix *Drosophila* Tiling 2.0R Arrays. Digital DNase I-Seq assays were performed as described previously[44], and Global Run-On library (GRO-Seq) data was generated as described previously[31]. Short RNA data was generated by ref. 30, and RNA-Seq data was generated by ref. 45. See ref. 46 for other modENCODE RNA-Seq data. The chromatin state models were generated as hidden Markov models (HMMs) of different histone marks. DHSs were identified as read density peaks significantly enriched relative to the genomic DNA control. Clustering of chromatin signatures was determined using the PAM algorithm.

Full Methods and any associated references are available in the online version of the paper at www.nature.com/nature.

1. modENCODE. Identification of functional elements and regulatory circuits by *Drosophila* modENCODE. *Science* doi:10.1126/science.1198374 (in the press).
2. Gerstein, M. B. *et al.* Integrative analysis of the *Caenorhabditis elegans* genome by the modENCODE project. *Science* doi:10.1126/science.1196914 (in the press).
3. Adams, M. D. *et al.* The genome sequence of *Drosophila melanogaster*. *Science* **287,** 2185–2195 (2000).
4. Clark, A. G. *et al.* Evolution of genes and genomes on the *Drosophila* phylogeny. *Nature* **450,** 203–218 (2007).
5. Hoskins, R. A. *et al.* Sequence finishing and mapping of *Drosophila melanogaster* heterochromatin. *Science* **316,** 1625–1628 (2007).
6. Tweedie, S. *et al.* FlyBase: enhancing *Drosophila* Gene Ontology annotations. *Nucleic Acids Res.* **37,** D555–D559 (2009).
7. Felsenfeld, G. & Groudine, M. Controlling the double helix. *Nature* **421,** 448–453 (2003).
8. Mendenhall, E. M. & Bernstein, B. E. Chromatin state maps: new technologies, new insights. *Curr. Opin. Genet. Dev.* **18,** 109–115 (2008).
9. Egelhofer, T. A. *et al.* An assessment of histone-modification antibody quality. *Nature Struct. Mol. Biol.* doi:10.1038/nsmb.1972 (5 December 2010).
10. Eissenberg, J. C. & Reuter, G. Cellular mechanism for targeting heterochromatin formation in *Drosophila*. *Int. Rev. Cell Mol. Biol.* **273,** 1–47 (2009).
11. Schwartz, Y. B. & Pirrotta, V. Polycomb complexes and epigenetic states. *Curr. Opin. Cell Biol.* **20,** 266–273 (2008).
12. Li, B., Carey, M. & Workman, J. L. The role of chromatin during transcription. *Cell* **128,** 707–719 (2007).
13. Liu, C. L. *et al.* Single-nucleosome mapping of histone modifications in *S. cerevisiae*. *PLoS Biol.* **3,** e328 (2005).
14. Barski, A. *et al.* High-resolution profiling of histone methylations in the human genome. *Cell* **129,** 823–837 (2007).
15. Larschan, E. *et al.* MSL complex is attracted to genes marked by H3K36 trimethylation using a sequence-independent mechanism. *Mol. Cell* **28,** 121–133 (2007).
16. Riddle, N. C. *et al.* Plasticity in patterns of histone modifications and chromosomal proteins in *Drosophila* heterochromatin. *Genome Res.* doi:10.1101/gr.110098.110 (in the press).
17. Anders, S. Visualization of genomic data with the Hilbert curve. *Bioinformatics* **25,** 1231–1235 (2009).
18. MacAlpine, D. M., Rodriguez, H. K. & Bell, S. P. Coordination of replication and transcription along a *Drosophila* chromosome. *Genes Dev.* **18,** 3094–3105 (2004).
19. Blumenthal, A. B., Kriegstein, H. J. & Hogness, D. S. The units of DNA replication in *Drosophila melanogaster* chromosomes. *Cold Spring Harb. Symp. Quant. Biol.* **38,** 205–223 (1974).
20. Ernst, J. & Kellis, M. Discovery and characterization of chromatin states for systematic annotation of the human genome. *Nature Biotechnol.* **28,** 817–825 (2010).
21. Misulovin, Z. *et al.* Association of cohesin and Nipped-B with transcriptionally active regions of the *Drosophila melanogaster* genome. *Chromosoma* **117,** 89–102 (2008).
22. Kagey, M. H. *et al.* Mediator and cohesin connect gene expression and chromatin architecture. *Nature* **467,** 430–435 (2010).
23. Deal, R. B., Henikoff, J. G. & Henikoff, S. Genome-wide kinetics of nucleosome turnover determined by metabolic labeling of histones. *Science* **328,** 1161–1164 (2010).
24. Henikoff, S., Henikoff, J. G., Sakai, A., Loeb, G. B. & Ahmad, K. Genome-wide profiling of salt fractions maps physical properties of chromatin. *Genome Res.* **19,** 460–469 (2009).
25. MacAlpine, H. K., Gordan, R., Powell, S. K., Hartemink, A. J. & MacAlpine, D. M. *Drosophila* ORC localizes to open chromatin and marks sites of cohesin complex loading. *Genome Res.* **20,** 201–211 (2010).
26. Visel, A. *et al.* ChIP-seq accurately predicts tissue-specific activity of enhancers. *Nature* **457,** 854–858 (2009).
27. Zinzen, R. P., Girardot, C., Gagneur, J., Braun, M. & Furlong, E. E. Combinatorial binding predicts spatio-temporal *cis*-regulatory activity. *Nature* **462,** 65–70 (2009).
28. Schwartz, Y. B. *et al.* Genome-wide analysis of Polycomb targets in *Drosophila melanogaster*. *Nature Genet.* **38,** 700–705 (2006).
29. Schwartz, Y. B. *et al.* Alternative epigenetic chromatin states of Polycomb target genes. *PLoS Genet.* **6,** e1000805 (2010).
30. Nechaev, S. *et al.* Global analysis of short RNAs reveals widespread promoter-proximal stalling and arrest of Pol II in *Drosophila*. *Science* **327,** 335–338 (2010).
31. Core, L. J., Waterfall, J. J. & Lis, J. T. Nascent RNA sequencing reveals widespread pausing and divergent initiation at human promoters. *Science* **322,** 1845–1848 (2008).
32. Wu, C. The 5′ ends of *Drosophila* heat shock genes in chromatin are hypersensitive to DNase I. *Nature* **286,** 854–860 (1980).
33. Wu, C., Bingham, P. M., Livak, K. J., Holmgren, R. & Elgin, S. C. The chromatin structure of specific genes: I. Evidence for higher order domains of defined DNA sequence. *Cell* **16,** 797–806 (1979).
34. Elgin, S. C. The formation and function of DNase I hypersensitive sites in the process of gene activation. *J. Biol. Chem.* **263,** 19259–19262 (1988).
35. Jin, C. *et al.* H3.3/H2A.Z double variant-containing nucleosomes mark 'nucleosome-free regions' of active promoters and other regulatory regions. *Nature Genet.* **41,** 941–945 (2009).
36. Hesselberth, J. R. *et al.* Global mapping of protein-DNA interactions *in vivo* by digital genomic footprinting. *Nature Methods* **6,** 283–289 (2009).
37. Heintzman, N. D. *et al.* Histone modifications at human enhancers reflect global cell-type-specific gene expression. *Nature* **459,** 108–112 (2009).
38. MacArthur, S. *et al.* Developmental roles of 21 *Drosophila* transcription factors are determined by quantitative differences in binding to an overlapping set of thousands of genomic regions. *Genome Biol.* **10,** R80 (2009).
39. Kim, T. K. *et al.* Widespread transcription at neuronal activity-regulated enhancers. *Nature* **465,** 182–187 (2010).
40. Filion, G. J. *et al.* Systematic protein location mapping reveals five principal chromatin types in *Drosophila* cells. *Cell* **143,** 212–224 (2010).
41. Bernstein, B. E. *et al.* A bivalent chromatin structure marks key developmental genes in embryonic stem cells. *Cell* **125,** 315–326 (2006).
42. Kanhere, A. *et al.* Short RNAs are transcribed from repressed polycomb target genes and interact with polycomb repressive complex-2. *Mol. Cell* **38,** 675–688 (2010).
43. Schuettengruber, B. *et al.* Functional anatomy of polycomb and trithorax chromatin landscapes in *Drosophila* embryos. *PLoS Biol.* **7,** e13 (2009).
44. Sekimata, M. *et al.* CCCTC-binding factor and the transcription factor T-bet orchestrate T helper 1 cell-specific structure and function at the interferon-γ locus. *Immunity* **31,** 551–564 (2009).
45. Cherbas, L. *et al.* The transcriptional diversity of 25 *Drosophila* cell lines. *Genome Res.* **21,** doi:10.1101/gr.112961.110 (in the press).
46. Gravely, B. R. *et al.* The developmental transcriptome of *Drosophila melanogaster*. *Nature* doi:10.1038/nature09715 (this issue).

Author Contributions P.V.K. performed most bioinformatic analysis. A.A.A., Y.B.S., A.M., N.C.R., E.L., A.A.G., T.G., D.L.-B., A.P. and G.S. generated data, directed by S.C.R.E., M.I.K., V.P. and G.H.K. The 30-state analysis was performed by J.E. and M.K., whereas M.Y.T., L.J.L., R.X., Y.L.J., R.W.P. and E.P.B. performed additional bioinformatic analysis. P.J.S., T.P.C., R.S., R.E.T. and J.A.S. generated and processed DHS data. D.M.M. helped with replication analysis. P.J.P. supervised all analysis. G.H.K. coordinated the entire project. P.V.K., G.H.K. and P.J.P. wrote the manuscript, with contributions from S.C.R.E., M.I.K., V.P., Y.B.S, N.C.R, A.A.A. and A.M.

METHODS

Growth conditions. ML-DmBG3-c2 cells were obtained from DGRC (https://dgrc.cgb.indiana.edu/), and S2-DRSC cells were from the DRSC (http://www.flyrnai.org/). All cell lines were grown to a density of ~5×10^6 cells ml^{-1} in Schneider's media (Gibco) supplemented with 10% FCS (HyClone). 10 μg ml^{-1} insulin was added to the ML-DmBG3-c2 media.

Antibodies. Antibodies are listed in Supplementary Table 1. Commercial antibodies against modified histones were tested by western blot for the lack of cross-reactivity with the corresponding recombinant histone produced in *Escherichia coli* and non-histone proteins from embryonic nuclear extracts. Antibody specificity was further assayed by western dot/slot blot against a panel of synthetic modified histone peptides. Only antibodies that showed <50% of total signal associated with non-histone proteins, and more than fivefold higher affinity for the corresponding histone peptide, were used in ChIP experiments.

The specificity of antibodies against chromosomal proteins was tested by western blots with nuclear extracts prepared from mutant flies or S2 cells subjected to RNAi knockdown[47]. An antibody was considered specific if it recognized a major band of expected mobility that was absent in the sample prepared from mutant flies, or diminished twofold or more after RNAi depletion. When possible, distributions of a chromosomal protein were mapped with two antibodies generated against different epitopes (see Supplementary Fig. 17). Data from chromatin proteins for which only one antibody was available were validated by comparison with published genomic distributions for a different component of the same complex, or to published genomic distributions generated with a different antibody.

ChIP and microarray hybridization. Crosslinked chromatin from cultured cells was prepared as described[28] with the following modifications. Before ultrasound shearing, cells were permeabilized with 1% SDS, and shearing was done in TE-PMSF (0.1% SDS, 10 mM Tris-HCl pH 8.0, 1 mM EDTA pH 8.0, 1 mM PMSF) using a Bioruptor (Diagenode) (2×10 min, 1×5 min; 30 s on, 30 s off; high power setting).

ChIP was performed as in ref. 28 and immunoprecipitated DNA was amplified using the whole genome amplification kit (WGA2, Sigma) according to the manufacturer's instructions (chemical fragmentation step was omitted). The amplified material was labelled and hybridized to *Drosophila* Tiling Arrays v2.0 (Affymetrix) as in ref. 28.

Processing of ChIP data. At least two independent biological replicates were assessed for each ChIP profile. The log$_2$ intensity ratios (*M* values) were calculated for each replicate. The profiles were smoothed using local regression (lowess) with 500 bp bandwidth, and the genome-wide mean was subtracted. The regions of significant enrichment were determined as clusters of at least 1 kb in length, with gaps no more than 100 bp where *M* value exceeds a statistically significant (0.1% false discovery rate (FDR)) enrichment threshold. The set of biological replicates was deemed consistent if the enriched regions from individual experiments had a 75% reciprocal overlap, or if at least 80% of the top 40% of the regions identified in each experiment were identified in the other replicate (before comparison the replicates were size-equalized by increasing the significance threshold for a replicate with more enriched sequence). The data from individual replicates were then combined using local regression smoothing, and used for all of the presented analysis, unless noted otherwise.

DNase I hypersensitivity. Digital DNase I-Seq assays were performed as described previously[44]. The sequenced reads were aligned to the Berkeley Drosophila Genome Project release 5 (BDGP.R5) genome assembly, recording only uniquely mappable reads. To detect DNase I hypersensitive sites, hotspot positions were identified based on a 300-bp scanning window statistic (Poisson model relative to 50 kb background density, *Z*-score threshold of 2), and peaks of read density were selected within the hotspots using randomization-based thresholding at 0.1% FDR. The set of high-magnitude DHSs analysed here (except for Supplementary Fig. 23) was identified as a subset of all peaks that show statistically significant enrichment over the normalized genomic DNA read density profile (using a 300-bp window centred around the peak, binomial model, with *Z*-score threshold of 3). This method controls for copy number variation and sequencing/mapping biases; however, it may also reduce the sensitivity of DHS detection. In the DHS chromatin profile clustering analysis (Fig. 5a, relevant Supplementary figures), DHSs found within 1 kb of another DHS were excluded if their enrichment magnitude (relative to genomic background) was lower (to avoid showing the same region more than once).

RNA sequencing. The preparation of RNA-Seq libraries and sequencing is described in ref. 45. The sequenced reads were aligned to the BDGP.R5 genome assembly and annotated exon junctions, recording only uniquely mappable reads. The RPKM (reads per kilobase of exonic sequence per million reads mapped) was estimated for each exon. The total transcriptional output of each annotated gene was estimated based on the maximum of all exons within the gene. The presented analysis uses log$_{10}$(RPKM+1) values unless otherwise noted.

GRO sequencing. Global Run-On library was prepared from S2 cells and sequenced as described[31]. The reads were aligned to the BDGP.R5 genome assembly, recording only uniquely mappable reads. The smoothed profiles of reads mapping to each strand were calculated using Gaussian smoothing ($\sigma = 100$ bp). The analysis uses log$_{10}$(d+1), where d is the smoothed density value.

Short RNA data processing. The short RNA data for S2 cells was generated by ref. 30, and was aligned and processed in the same way as the GRO-Seq data.

Chromatin state models. To derive a 9-state joint chromatin state model for S2 and BG3 cells (Fig. 1a), the genome was first divided into 200-bp bins, and the average enrichment level was calculated within each bin based on unsmoothed log$_2$ intensity ratio values taking into account individual replicates, using all histone enrichment profiles and PC to discount the genome-wide difference in S2 H3K27me3 profiles. The bin-average values of each mark were shifted by the genome-wide mean, scaled by the genome-wide variance, and quantile-normalized between the two cells. The hidden Markov model (HMM) with multivariate normal emission distributions was then determined from the Baum–Welch algorithm using data from both cell types, and 30 seeding configurations determined with *K*-means clustering. States with minor intensity variations (Euclidian distance of mean emission values <0.15) were merged. Larger models (up to 30 states) were examined, and the final number of states was chosen for optimal interpretability.

An extensive discrete chromatin state model (Supplementary Fig. 11) was calculated as described in ref. 20. The model was trained using a 200-bp grid with binary calls (enriched/not enriched). The binary calls were made based on a 5% FDR threshold determined from ten genome-wide randomizations for each mark. For H1, H4 and H3K23ac regions of significant depletion rather than enrichment were called.

Regions of enrichment for individual marks. To determine contiguous regions of enrichment for individual marks, a three-state HMM was used, with states corresponding to enriched, neutral and depleted profiles (normally-distributed emission parameters: ($\mu = [-0.5\ 0\ 0.5]$, $\sigma^2 = 0.3$). The enriched regions were determined from the Viterbi path. The HMM segmentation was applied to unsmoothed *M* value data taking into account individual biological replicates. The genes were clustered based on the combinatorial pattern of occurrence of enriched regions (coding exons and state panels were not used for clustering).

Classification of enrichment profiles. Clustering of chromatin signatures around TSSs (Fig. 4a), PREs (Fig. 4b) and DHSs (Fig. 5a and relevant Supplementary Information sections) was determined using the Partitioning Around Medoids algorithm. For clustering, each profile was summarized with average values within bins spanning ±2-kb regions. One-hundred-base-pair bins were used for the central ±500-bp region, 300-bp bins outside.

47. Clemens, J. C. *et al.* Use of double-stranded RNA interference in *Drosophila* cell lines to dissect signal transduction pathways. *Proc. Natl Acad. Sci. USA* **97,** 6499–6503 (2000).